Ultra-Compact H II Regions and the Early Lives of Massive Stars

M. G. Hoare
University of Leeds

S. E. Kurtz and S. Lizano
Universidad Nacional Autónoma de México - Morelia

E. Keto
Harvard University

P. Hofner
New Mexico Institute of Technology and National Radio Astronomy Observatory

We review the phenomenon of ultra-compact H II regions (UCHIIs) as a key phase in the early lives of massive stars. This most visible manifestation of massive star formation begins when the Lyman continuum output from the massive young stellar object becomes sufficient to ionize the surroundings from which it was born. Knowledge of this environment is gained through an understanding of the morphologies of UCHII regions and we examine the latest developments in deep radio and mid-IR imaging. SPITZER data from the GLIMPSE survey are an important new resource in which PAH emission and the ionizing stars can be seen. These data provide good indications as to whether extended radio continuum emission around UCHII regions is part of the same structure or due to separate sources in close proximity. We review the role played by strong stellar winds from the central stars in sweeping out central cavities and causing the limb-brightened appearance. New clues to the wind properties from stellar spectroscopy and hard X-ray emission are discussed. A range of evidence from velocity structure, proper motions, the molecular environment and recent hydrodynamical modeling indicates that cometary UCHII regions require a combination of champagne flow and bow shock motion. The frequent appearance of hot cores, maser activity and massive young stellar objects (YSOs) ahead of cometary regions is noted. Finally, we discuss the class of hyper-compact H II regions or broad recombination line objects. They are likely to mark the transition soon after the breakout of the Lyman continuum radiation from the young star. Models for these objects are presented, including photo-evaporating disks and ionized accretion flows that are gravitationally trapped. Evolutionary scenarios tracing young massive stars passage through these ionized phases are discussed.

1. INTRODUCTION

The time when newly formed massive stars begin to ionize their surroundings is one of the energetic events that underlines their important role in astrophysics. As they evolve, the copious amounts of UV radiation and powerful stellar winds they produce have a profound effect on the surrounding interstellar medium. Their early lives are spent deeply embedded within dense molecular cores whose high column densities absorb the optical and near-IR light from the young stars, shielding them from view. One of the first observable manifestations of a newly formed massive star is the radio free-free emission of the H II region surrounding the star. Since only the most massive stars produce significant radiation beyond the Lyman limit, embedded H II regions are a unique identifier of high mass star formation.

The absorption of the UV and optical radiation by dust, both in and outside the newly formed nebula, heats the grains to temperatures that range from the sublimation temperature close to the star to interstellar temperatures in the surrounding molecular cloud. Owing to the high luminosity of the massive stars, H II regions are some of the strongest infrared sources in the galaxy. Similar to the radio emission, the thermal IR radiation is little affected by extinction. Thus the combination of the radio and IR wave bands allows us to peer deep into the star forming clouds to study the processes of star formation within.

The youngest massive stars are associated with the smallest H II regions. These are the ultra-compact H II regions (UCHII) and the newly identified class of hypercompact (HCHII) regions. UCHII regions were first distinguished from merely "compact" H II regions around 25 years ago, and came to be defined observationally (*Wood and Churchwell*, 1989a) as those regions with sizes ≤ 0.1 pc, densities $\geq 10^4$ cm^{-3}, and emission measures $\geq 10^7$ pc cm^{-6}. Since then, hundreds of UCHII regions

with these general properties have been found. Whilst the division of H II regions into different degrees of compactness may be a convenient label, for the larger objects at least, it is likely to have little physical significance. Once in the expansion phase, the physics of their dynamics probably stays the same until the molecular material is cleared away and the OB star joins the field population. Of greater interest are the smallest H II regions, as they more to tell us about the process of massive star formation. The ionized gas within the UCHII and HCHII regions not only reveals properties of the stars themselves, but also lights up the immediate surroundings to allow investigations of the density distribution and environment into which the massive stars are born. The external environment has a profound influence on the evolution of the H II regions.

The properties of UCHII regions and their immediate precursors have been reviewed previously by *Churchwell* (2002) and *Kurtz et al.* (2000). In this review we concentrate on more recent developments in the field of UCHII and HCHII regions. These include new theories of massive star forming accretion flows and the new views of UCHII regions opened up by infrared studies on large ground-based telescopes and the SPITZER satellite. The SPITZER GLIMPSE survey has covered a large part of the inner galactic plane at unprecedented spatial resolution and depth in the 4-8 μm region where there is a local minimum in the extinction curve. High resolution X-ray studies with *Chandra* are also beginning to bear on the problem. Together these promise great new insights into how OB stars are formed and interact with their environment.

2. ULTRA-COMPACT H II REGIONS

2.1 Morphologies

The morphologies of UCHII regions are important since they yield clues to the state of the surrounding medium relatively soon after a massive star has formed. The common appearance of a regular morphology indicates that there are ordered physical processes occurring during massive star formation rather than just stochastic ones.

As part of their pioneering high resolution radio surveys of massive star forming regions *Wood and Churchwell* (1989a) developed a morphological classification scheme for UCHII regions. Together with *Kurtz et al.* (1994), they found that 28% of UCHII regions are spherical, 26% cometary, 26% irregular, 17% core-halo and 3% shell. The significant numbers of unresolved sources have been omitted here, since nothing can be said about their morphology. *Walsh et al.* (1998) studied a sample of southern UCHII regions and classified most of their sources as either cometary (43%) or irregular (40%) after omitting the unresolved ones. As pointed out by *Wood and Churchwell*, many of the sources classified as spherical do reveal ordered morphology when observed at higher spatial resolution. Examples are M17-UC1, which was shown to be cometary (*Felli et al.*, 1984) and G28.20-0.04, which is shell-like (*Sewilo et al.*, 2004) (see Fig. 7). If the spherical sources of earlier studies were also discounted, then the proportion of cometaries in the well-resolved objects would be similar to that from *Walsh et al.*

As *Wood and Churchwell* forewarned, radio interferometric observations have a limited range of spatial scales that they are sensitive to. The larger objects can quickly become over-resolved and break up into irregular sources. The snapshot nature of observations necessary to investigate significant numbers of sources also limits the dynamic range. For cometary objects this often means that at high resolution only the dense material at the head is seen and the full extent of the much weaker emission in the tail is not. Even for relatively simple objects like the archetypal cometary UCHII region, G29.96-0.02, the complete radio continuum picture is only fully revealed by time consuming deep, multi-configuration observations (*Fey et al.*, 1995).

The recent radio studies by *De Pree et al.* (2005) also address this point. They have conducted deep, multi-configuration studies of two regions of intense massive star formation, W49A and Sgr B2, where nearly 100 UCHII regions are found. These radio data had good spatial and dynamic range leading *De Pree et al.* to reassess the morphological classes. They classify about one third of their sources as 'shell-like', after omitting the unresolved fraction. At least half of these are very asymmetric and could just as easily be classified as cometary. This would take the total cometary fraction to over a third in that sample. The high dynamic range of the *De Pree et al.* data also led them to drop the core-halo class and instead attempt to ascertain the shape of the compact and extended emission separately. These sources often appear to be a superposition of a compact source on a different, more extended source. They also detect a significant population of UCHII regions elongated along one axis. Following *Churchwell* (2002) they classify these regions as bipolar. It is not yet clear whether the detection of these bipolar sources is due to the better quality radio imaging or the more extreme pressure in these two environments compared to the general galactic population.

Imaging in the infrared is sensitive to all spatial scales at once, from the resolution limit up to the total size of the image. This could be several orders of magnitude of spatial dynamic range as long as the image is sensitive enough to pick up very extended, low surface brightness emission. Therefore, IR imaging can in principle overcome some of the limitations of radio interferometric snapshot data for morphological classification, although it also comes with its own disadvantages. In the near-IR, the continuum emission from UCHII regions is mostly made up of bound-free and free-free emission from the nebular gas. There are also minor contributions from scattered light, emission from very hot grains and non-thermal equilibrium emission from very small grains. Hence, near-IR images should show the same morphology as the radio, apart from the effect of intervening extinction. An example of this is seen in the near-IR image of G29.96-0.02 by *Fey et al.*, where the nebular continuum looks just like their deep multi-configuration radio

map. However, in general the extinction in the near-IR is often too high and renders the UCHIIs invisible or cut through by dust extinction lanes.

Moving into the thermal IR reduces the total extinction, mostly eliminates scattering by the dust and the UCHII regions become much brighter. The interstellar dust grains are heated by a combination of direct stellar radiation near the star and Lα photons resonantly scattering in the ionized zone (e.g., *Natta and Panagia*, 1976 and *Hoare et al.*, 1991). The latter process means that the dust grains never drop below temperatures of a few hundred Kelvin throughout the nebula and thus emit strongly in the mid-IR. As such, the intrinsic mid-IR morphology is similar to that seen in the radio, but again heavy extinction can intervene.

The advent of a new generation of mid-IR cameras on large telescopes has yielded high quality mid-IR images of a number of UCHII regions. In many cases the mid-IR and radio morphology are in good agreement. Recent examples include W49A South (*Smith et al.*, 2000), G29.96-0.02 (*De Buizer et al.*, 2002a), NGC6334F (*De Buizer et al.*, 2002b), W3(OH) (*Stecklum et al.*, 2002), and K3-50A (*Okamoto et al.*, 2003) and several sources observed by *Kraemer et al.* (2003). In the cometary G9.62+0.19B there are even signs of a bright spot near the expected location of the exciting star due to direct stellar heating (*De Buizer et al.*, 2003 and *Linz et al.*, 2005).

There are other objects, however, where a large extinction, even at 10 and 20 μm, greatly attenuates the mid-IR emission. A good example is G5.89-0.39, where the heavy extinction in the near-IR obscures the southern half of the radio source in the N and Q bands, consistent with the large column density measured in the millimetre continuum (*Feldt et al.*, 1999). *De Buizer et al.* (2003, 2005) and *Linz et al.* (2005) show other instances where the mid-IR morphology does not follow that of the radio continuum. The most likely reason for this is extinction, which, due to the silicate features, is still high in the ground-based mid-IR windows. Indeed, the extinction at these wavelengths is only about half of the value in the K-band (*Draine*, 2003).

Observations by the SPITZER satellite now offer a whole new IR perspective on UCHII regions, in particular through the GLIMPSE survey of a large fraction of the inner Galactic Plane (*Benjamin et al.*, 2003). The 4-8 μm range of the IRAC instrument has extinction values lower than both the near- and ground-based mid-IR windows, bottoming out around the 5.8 μm channel (*Indebetouw et al.*, 2005). At these wavelengths one can expect to see some emission from the hot grains in thermal equilibrium near the exciting star. However, the IRAC filters at 3.6, 5.8 and 8.0 μm are dominated by strong PAH features from the UCHII regions. The PAH emission is strong in the photon-dominated regions (PDRs) that lie in a thin shell of neutral gas just outside the ionization front. In directions in which the H II region is ionization bounded, the PAH emission is expected to form a sheath around the nebula. If there are directions where ionizing photons can escape, the PAHs will be destroyed (*Girad et al.*, 1994).

An example for a cometary UCHII region is shown in Fig. 1 (left) where the 8 μm emission closely follows the radio emission around the head and sides, but is absent in the tail direction which is likely to be density bounded. Possibly unrelated clumps and filaments can be seen in the vicinity, so caution must be exercised when interpreting the SPITZER images; information from other wavelengths, especially the radio, is also needed. Nevertheless, the uniformity and coverage of the GLIMPSE dataset makes it very useful for studies of UCHII regions. Its resolution and sensitivity can in principle yield new insights into the morphologies of UCHII regions, notwithstanding the caveats mentioned above.

Hoare et al., (in prep.) are carrying out mid-IR morphological classification utilising the GLIMPSE dataset. They are using a sample of massive young stars colour-selected from the lower resolution mid-IR survey by the MSX satellite (*Lumsden et al.*, 2002). These have been followed-up with a variety of ground-based observations, including high resolution radio continuum observations to identify the UCHII regions and massive YSOs (*Hoare et al.*, 2004; www.ast.leeds.ac.uk/RMS). Preliminary findings indicate that the proportion of cometary objects is higher than in previous radio studies. Fig. 1 (right) shows an example where the radio image is barely resolved and yet the GLIMPSE 8 μm image shows a 'horseshoe' shaped nebula wrapped around the radio source as expected for PAHs in a PDR. However, the structure is open to the NNE suggesting that the UCHII region is not ionization bounded in that direction. Although it does not have the classic parabolic shape of a cometary, it is suggestive of a champagne flow away from the dense molecular cloud seen in extinction ahead of the object. Other data are needed to confirm such an interpretation. A star is seen in the centre of the nebula in the 3.6 and 4.5 μm GLIMPSE images and is likely to be the exciting source. This demonstrates that the IRAC wavelength range can address many aspects of UCHII regions.

Kurtz et al. (1999) found that many UCHII regions, when observed at lower angular resolution, show extended, diffuse emission in addition to the ultra-compact component. The radio morphologies suggested a physical connection between the UCHII region and the extended component for a significant fraction of their sources. *Kim and Koo* (2001), using a different sample, made radio recombination line observations of UCHIIs with extended emission. The line velocities of the ultra-compact and extended gas were nearly equal, supporting the idea of a physical relationship between the two components. *Ellingsen et al.* (2005) searched for extended emission in eight southern UCHIIs with associated methanol masers. They found a lesser degree of extended emission than reported for the random UCHII sample of *Kurtz et al.* Methanol masers may trace earlier stages of UCHII regions, hence the lesser degree of extended emission in the *Ellingsen et al.* sample may reflect the relative youth of those regions.

As pointed out by *Kurtz et al.* (1999) in many cases it is difficult to assess from the radio data whether the ex-

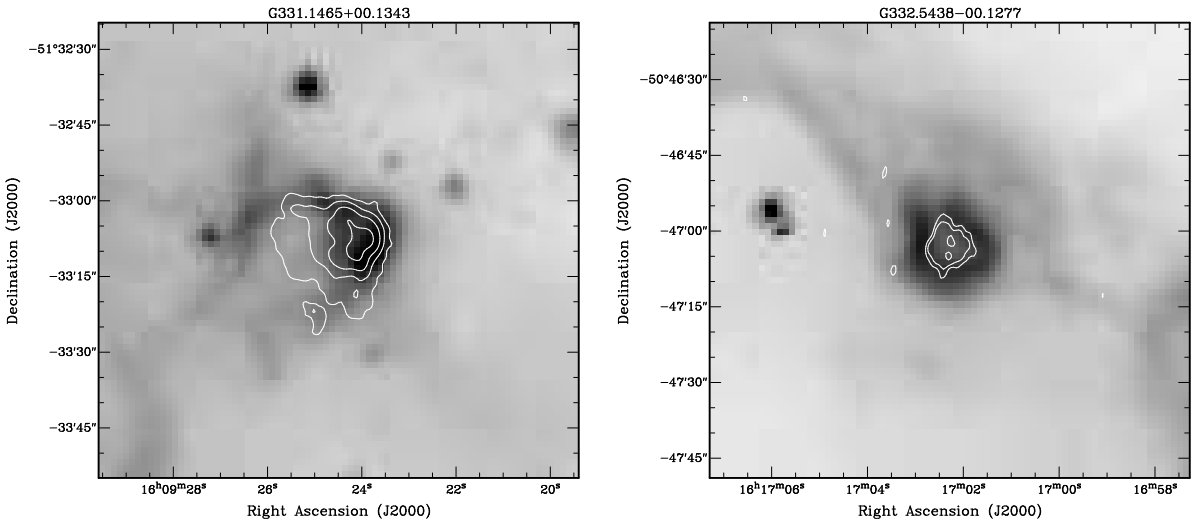

Fig. 1.— Left: 8.0 μm GLIMPSE image of G331.1465+00.1343 overlaid with contours of the 5 GHz radio continuum emission from ATCA with a noise level of 0.2 mJy per beam at a resolution of about 3 $''$ The object has a clear cometary morphology seen in both the radio and mid-IR image. Right: Same for G332.5438-00.1277. Note the 'horseshoe' shaped IR emission that is open to the NNE similar to cometary objects and not revealed by the barely resolved radio image. For both sources there is a darker region ahead of the object in the 8.0 μm image indicating extinction due to dense molecular cloud material From *Busfield (2006)*, PhD thesis, University of Leeds.

tended emission is a coherent structure excited by the same star(s). IR images can often clarify the situation; the case of G031.3948-0.2585 (IRAS 18469-0132) is shown in Fig. 2. The lower resolution radio map of *Kurtz et al.* (1999) shows connected radio emission over two arcminutes. In the IR image it looks more like a complex of several different sources. The cometary, with a size of about 15$''$ in the high resolution radio image, is seen along with IR counterparts to the two radio point sources. However, the diffuse radio emission, seen extending to the east and north in the low resolution radio map, appears to be due to a combination of another larger cometary with its tail pointing north-east and an ionized bright-rimmed cloud type structure running to the south and east of the two cometary objects. Spectrophotometric identification of the individual exciting stars, together with high spatial and dynamic radio continuum and line observations are needed to confirm the picture in detail.

2.2 Molecular Environment

In this section we examine the molecular environment within which UCHII regions exist, and in particular, that of cometary regions. Unfortunately, the typical spatial resolution of single-dish millimetre line observations is usually insufficient to resolve UCHII regions from associated star formation activity and the molecular cores where they reside. Higher resolution data on the molecular environment can be obtained with millimetre interferometry. However, most studies of the environs of UCHII regions have naturally tended to concentrate on those with associated hot cores. Although this benefits high mass star formation studies in general, it is not so useful in the search for a full understanding of UCHII region physics, a key ingredient of which is the ambient density distribution. The presence of a hot core with its own associated infall and possibly outflow in close proximity to the UCHII hampers a clear view of the molecular environment into which the older UCHII region was born.

In single-dish studies *Hofner et al.* (2000) used optically thin $C^{17}O$ transitions to determine that the molecular clumps in which UCHII regions reside are typically about 1 pc is size with densities of 10^5 cm^{-3} and temperatures of 25 K. In their survey of ^{13}CO and CS transitions, *Kim and Koo* (2003) found that the UCHII region is usually located right at the peak of the molecular line emission. When they did resolve clear density and velocity structure in the molecular gas, the pattern was consistent with a champagne flow.

Somewhat higher resolution information on the density distribution is available from sub-millimetre dust continuum emission maps (*Mueller et al.*, 2002). These show very centrally condensed clouds centred on the UCHII regions themselves, but if there is an offset of the peak density then it is usually ahead of the cometary apex. Using the sub-millimetre dust continuum will give a more centrally peaked distribution than a pure column density tracer, as the warm dust in and around the nebula will enhance the sub-millimetre emission. *Hatchell and van der Tak* (2003) examined the more extended sub-millimetre continuum emission around UCHII regions and found that the average radial density distribution derived was consistent with the r$^{-1.5}$ expected for free-fall collapse.

About half of all UCHII regions are associated with

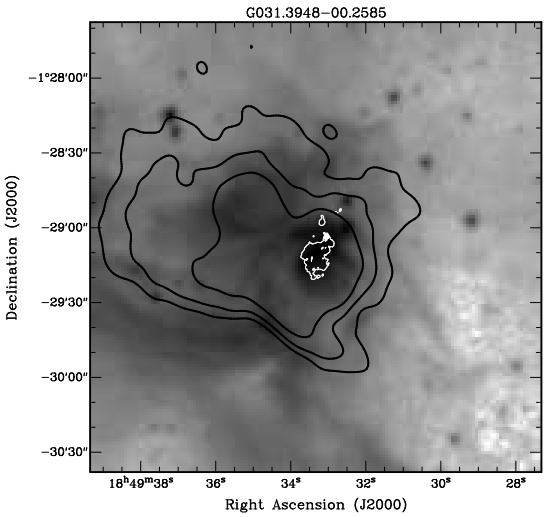

Fig. 2.— GLIMPSE 8 μm image of G031.3948-00.2585 (IRAS 18469-0132). Overlaid in thick black contours is the 3.6 cm data from VLA D configuration observations and in thin white contours the VLA B configuration data also at 3.6 cm. Radio data is from *Kurtz et al.* (1999). D array contours are at 1, 2 and 4 mJy per beam and then switch to the B array contours at 0.5 mJy per beam up to the peak. The IR image is more suggestive of a collection of separate UCHIIs and bright-rimmed clouds than a single source responsible for the compact and extended emission.

warm molecular gas as evidenced by highly excited NH_3 (*Cesaroni et al.*, 1992), CS (*Olmi and Cesaroni*, 1999), methanol masers (*Walsh et al.*, 1998) or other molecular tracers of the early hot core phase (*Hatchell et al.*, 1998). Higher resolution data showed that these hot cores were usually spatially offset from the UCHII regions by a few arcseconds (*Cesaroni et al.*, 1994). Where these are associated with cometary regions then the hot cores are always located ahead of the apex. Many cometary regions have been found to show signs of earlier stages of massive star formation such as maser sources or massive YSOs as well as hot cores in the dense regions a few arcseconds ahead of the cometary region (e.g., *Hofner et al.*, 1994; *Hofner and Churchwell*, 1996).

G29.96-0.02 is again a good case study. Interferometric observations of ^{13}CO 1-0 and C^{18}O 1-0 by *Pratap et al.* (1999) and *Olmi et al* (2003) reveal gas densities of 5×10^5 cm^{-3}. The density peaks just in front of the cometary H II region, at the location of the hot core. *Maxia et al.* (2001) found blue-shifted CO and HCO^+ 1-0 emission in the tail region and HCO^+ 1-0 in absorption, redshifted with respect to the main cloud at the head. They interpreted these motions as infall onto the hot core.

Fig. 3 shows a high resolution observation of the dense molecular gas associated with the cometary region G12.21-0.10. The molecular gas lies just in front of the cometary ionisation front. Observations of the NH_3 (2,2) line show that a hot core is present, coincident with a collection of water masers showing that star formation activity is occurring (*de la Fuente et al.*, in prep.). Recently these hot cores in the vicinity of UCHII regions have been detected in the mid-IR via their warm dust emission (*De Buizer et al.*, 2002a, 2003 and *Linz et al.*, 2005). Fig. 3 shows the first mid-IR detection of such an object ahead of the G29.96-0.02 cometary region.

In the few cases where a cometary object without obvious interference from a nearby hot core or massive young stellar object has been studied at high resolution, dense gas surrounding the head of the cometary structure has been found. Maps of W3(OH) in dense gas tracers such C^{18}O and CH_3OH (*Wyrowski et al.*, 1999) reveal an arc of emission wrapped around the western end of the UCHII region, which has a champagne flow to the east (*Keto et al.*, 1995). Similarly, high resolution observations of G34.24 by *Watt and Mundy* (1999) show C^{18}O 1-0 emission enveloping the head of this cometary region, whilst the traditional hot core tracer, methyl cyanide, peaks up right on the apex of the cometary region. *Watt and Mundy* interpret this emission as arising from dense molecular gas externally heated by the UCHII region rather than internally heated by a young massive star. The interpretation of molecular line emission close to the PDR around an UCHII region is complicated by the many excitation and chemical effects that are likely to be at work.

An alternative probe of dense molecular gas surrounding UCHII regions is to use molecular lines in absorption against the strong continuum background. This gives additional constraints due to the particular geometry necessary to generate them. The H_2CO lines at 2 and 6 cm have been observed at high resolution in absorption against W3(OH) and W58 C1 (*Dickel and Goss*, 1987; *Dickel et al.*, 2001). Both of these objects have a cometary structure and the H_2CO line optical depth maps of both objects show peaks consistent with the densest gas being located at the head of the cometary region. Total gas densities of 6×10^4 cm^{-3} were derived from the strengths of the absorption lines. The authors interpret other details in the line structure as arising from possible outflows from other sources in these regions.

Very high spatial resolution absorption line studies have been achieved with the NH_3 lines at 23 GHz. *Sollins et al.* (2004) found evidence of spherical infall together with some rotation in G10.6-0.4. A multi-transition study of G28.20-0.04 (*Sollins et al.*, 2005) revealed complex motions interpreted as a combination of toroidal infall and outflowing shell. These two H II regions fall into the hypercompact category (see Section 3).

Lines that arise in the PDR can probe the conditions and kinematics in the neutral material. Carbon radio recombination lines are particularly useful as they can be compared to the ionized gas traced by hydrogen and helium recombination lines. *Garay et al.* (1998b) and *Gómez et al.* (1998) observed these lines towards cometary objects and found that the spatial distribution and velocity of the carbon lines are consistent with an origin in a PDR around objects undergoing a champagne flow. The carbon lines are signifi-

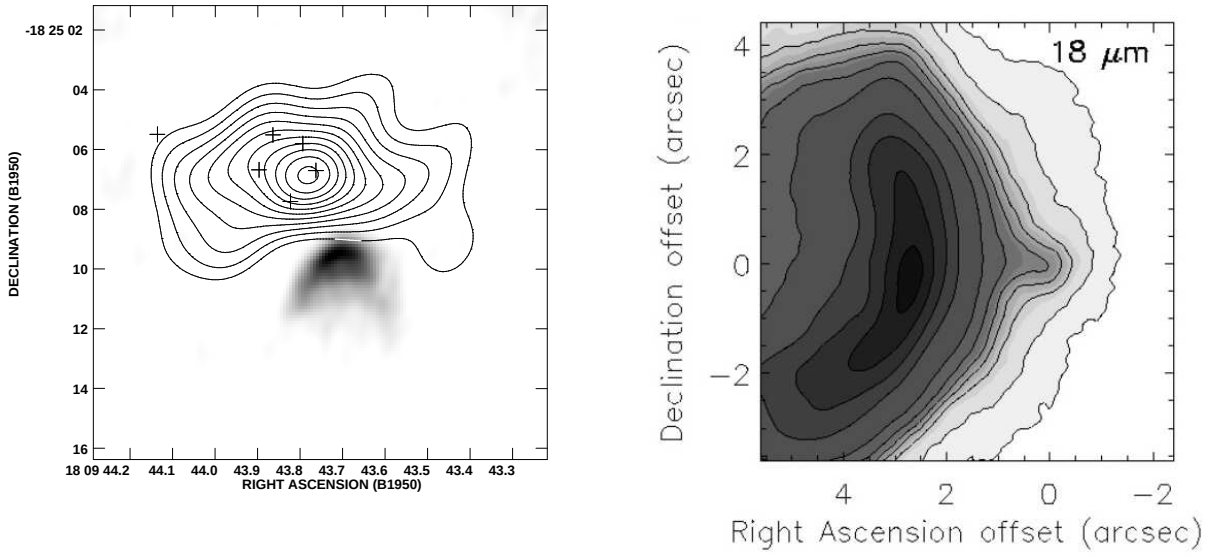

Fig. 3.— Left: High resolution map of the CS 2-1 emission (contours) tracing the dense molecular gas ahead of the cometary UCHII region G12.21-0.10 (radio continuum image in grey-scale). Crosses mark water masers. From *de la Fuente et al.*, in preparation. Right: 18 μm image of G29.96-0.02 showing the detection of the hot core located about 2 arcseconds in front of the cometary arc of the UCHII region. From *De Buizer et al.* (2002a).

cantly enhanced by stimulated emission and therefore arise predominately from the near side in front of the continuum, and hence give more specific insight into the velocity structure. *Roshi et al.* (2005a) used this fact to deduce that the PDR region in the cometary object G35.20-1.74 is moving into the cloud at a few km s^{-1} by comparison with the ambient molecular cloud velocity. *Lebrón et al.* (2001) report a comprehensive study of a cometary region, G111.61+0.37, using a combination of atomic hydrogen 21 cm emission and absorption components related to ionized and molecular lines. They demonstrated that the atomic gas exhibits a champagne flow like the ionized gas, but at significantly slower velocities, consistent with entrainment.

2.3 Stellar Winds

If we are to understand the nature of UCHII regions we first need a sound knowledge of the OB stars that excite them and their stellar winds. Due to the heavy extinction, optical and UV spectroscopic diagnostics are not available. Even for the objects that are visible in the near-IR when the extinction is low enough it is usually difficult to see them because of the very strong nebular continuum emission. One of the few stars that is clearly visible at 2 μm is the one that powers G29.96-0.02. *Martín-Hernández et al.* (2003) used the VLT to take an intermediate resolution K-band spectrum of the star building on previous work by *Watson et al.* (1997). By comparison with spectra of known spectral types from the field, they deduced that it was an O5-6V, and argued that this was consistent with other estimates of the spectral type. More importantly, the spectrum is consistent with field stars which argues that the stellar wind should also have properties similar to the well-studied radiation driven OB star winds. Hence, the action of a strong wind moving at a few thousands of km s^{-1} has to be an ingredient of any model of expanding UCHII regions.

The indirect information on the radiation output from the central stars via the study of the excitation of the nebulae has been put on a much firmer basis as a result of ISO spectroscopy of a large sample. *Martín-Hernández et al.* (2002) find a consistent picture whereby the metallicity gradient in the Galaxy can explain the excitation gradient due to the hardening of the stellar radiation field. However, progress is still required on the stellar atmosphere models to derive the exact stellar parameters. The use of the near-IR He I pure recombination lines can also help constrain the stellar parameters (*Lumsden et al.*, 2003). It should now be possible to combine the new spatially resolved mid-IR imaging with multi-dimensional dusty photo-ionization modelling including PAHs to determine the dust-to-gas ratio inside UCHII regions. This is crucial to finding the fraction of Lyman continuum photons absorbed by the dust which at present bedevils the use of radio to IR luminosities in constraining the stellar effective temperature.

There is an urgent need to find and conduct detailed direct studies of the exciting stars from a range of UCHII regions. *Bik et al.* (2005) have studied the spectra of many objects found in the vicinity of UCHII regions. However these were either OB stars in a cluster associated with, but not powering the UCHII region, or the UCHII region itself where the spectrum is dominated by the nebular continuum and not the star. To make progress, higher spatial resolution is required to pick the star out of the nebular light. *Alvarez*

et al. (2004) present a start down this road with near-IR adaptive optics imaging of several UCHII regions. Higher Strehl ratios on larger telescopes will be needed to carry out the high spatial and spectral resolution observations to classify the exciting stars. The speckle imaging of K3-50A by *Hoffmann et al.* (2004) shows the promise of such techniques.

Another new line of evidence that can give insights into the stellar winds in the centres of UCHII regions comes from X-ray observations. Hard X-ray sources are now routinely found in high mass star-forming regions. *Hofner et al.* (2002) made a study of the W3 region using the *Chandra X-ray Observatory* and found X-ray point sources coincident with many of the OB stars powering the more evolved H II regions, but also at the centres of some ultra-compact regions. The point-like emission from the visible stars in the evolved regions, which are not likely to be accreting, probably arises in shocks within a radiatively driven stellar wind. This could also be the case for the more compact sources, but accretion shocks or wind-nebula interactions are also possible. The diffuse X-ray emission arising from the very hot post-shock region where the stellar wind interacts with the surrounding UCHII region should fill the wind-blown cavity. Such diffuse emission is seen on much larger scales where clusters of OB stars excite a large complex such as M17 (see the chapter by *Feigelson et al.*). The indirect effect of X-ray emission in UCHII regions is the generation of a partially ionized layer just outside the nebula due to the penetration of hard photons into the neutral material. *Garay et al.* (1998a) observed narrow H I radio recombination line components, which they ascribed to X-ray heating.

If the wind-nebula interaction can be detected in diffuse X-rays in UCHII regions, it would in theory give an independent measure of the strength of the wind. However, the modelling of this interaction and its X-ray emission is far from straightforward. The evolution of wind driven regions expanding into a high pressure ambient medium was studied numerically by *García-Segura and Franco* (1996) who showed that the swept-up shells of ambient gas suffered a strong thin-shell instability producing "elephant-trunks" and cometary globules in the shocked stellar wind. In these models, a hot bubble of shocked stellar wind drives the expansion of a swept-up shell where the ionization front is trapped.

Comeron (1997) made some initial calculations in the context of stellar winds in a champagne flow scenario. More recently, *González-Avilés et al.* (2005) studied the evolution of an H II region driven by a strong stellar wind blowing inside a logatropic cloud in gravitational collapse toward the central star. They included thermal conductivity which reduces the shocked stellar wind cooling time by several orders of magnitude (*Shull*, 1980). The tangential magnetic fields will suppress the thermal conduction in the direction perpendicular to the magnetic field direction. Nevertheless, the morphology and strength of magnetic fields is unknown. Thus, the magnitude of the thermal conductivity coefficient, κ, was used as a free parameter. They found that only models with the full thermal value of κ were compatible with the hard X-ray luminosities observed in the W3 sources (10^{-3} $L_{\odot}$) by *Hofner et al.* (2002). For this value, thermal conductivity cools the hot region of shocked stellar wind and the shells of swept-up gas are driven by the momentum of the stellar wind. The hot shocked wind is also in a very thin shell and would predict emission on 0.1 pc scales that would easily be resolved by *Chandra*, which was not the case for the W3 sources. Much deeper observations of this and other massive star forming regions are being obtained and these may reveal the diffuse X-ray emission that will fully unlock this new insight into the effect of strong stellar winds in UCHII regions.

2.4 Dynamical Picture

As reviewed by *Churchwell* (1999), many models have been put forward to explain the morphologies and long lifetime of UCHIIs. *Wood and Churchwell* (1989b) were the first to argue that the sheer numbers of objects with IR colours like UCHII regions implies a lifetime of order 10^5 years rather than the simple dynamical lifetime of 10^4 years. This has since been criticised by several studies (*Codella et al.*, 1994; *Ramesh and Sridharan*, 1997; *van der Walt*, 1997; *Bourke et al.*, 2005), but nevertheless many models attempted to include ways of lengthening the lifetime of the phase. These included using thermal pressure to confine the expansion (*De Pree et al.*, 1995), although this was claimed by *Xie et al.* (1996) to predict too high an emission measure and they appealed to turbulent pressure instead. Another way is to continuously introduce neutral material to the ionized region. In mass-loading models by *Dyson et al.* (1995), *Lizano et al. 1996* and *Redman et al.* (1998) the ablation of neutral clumps sets up a recombination front structure. These models predict mainly double-peaked line profiles that are not observed. Magnetic fields may also impede the advance of ionisation fronts (*Williams et al.*, 2000) and require sensitive measurements of the field strength and geometry to test them.

For cometary objects, the bow shock model, whereby the stellar wind from an OB star moving through a uniform medium sets up a parabolic standing shock, also continuously feeds neutral material into the nebula (*Mac Low et al.*, 1991). Several high resolution radio recombination line studies of the dense gas at the head of cometary regions, and G29.96-0.02 in particular, observed a velocity structure that was claimed to support the bow shock model (*Wood and Churchwell*, 1991 and *Afflerbach et al.*, 1994). These pure bow shock models required the star to be moving at velocities of about 20 km s^{-1} to impart sufficient velocity structure into the gas. This is much higher than typical members of young OB star clusters, which have velocity dispersions of only a few km s^{-1} (e.g., *Sicilia-Aguilar et al.*, 2005). Of course, there exists a class of runaway OB stars that do have much higher proper motions, probably resulting from dynamical ejections (*Hoogerwerf et al.*, 2001 and see also *Gómez et al.*, 2005). However, these only make up a small

fraction of all OB stars (*Gies*, 1987; *de Wit et al.*, 2005). The velocity dispersion of young clusters where the potential is still dominated by gas will be higher. *Franco et al.* (2006) have recently carried out numerical simulations of UCHII regions in which the exciting star is moving with speeds of up to 13 km s^{-1} down a density gradient surrounding a hot core. They identify these stellar speeds as being consistent with viral motion due to the gravitational field of the hot core. Their motivation was to explain the occurrence of both compact and extended emission if due to a single ionising source (see Section 2.1.2).

Lower spatial resolution radio recombination line studies (e.g., *Garay et al.*, 1994; *Keto et al.*, 1995) that are sensitive to more extended emission in the tail of cometary objects, indicate fbwing motions consistent with the blister and champagne fbw models (*Israel*, 1978; *Yorke et al.*, 1983). Near-IR long-slit spectroscopy also showed that the velocity structure in the Brγ line in G29.96-0.02 was not consistent with a pure bow shock picture (*Lumsden and Hoare*, 1996, 1999). The same velocity structure was recently recovered by *Zhu et al.* (2005) using long-slit echelle observations of the 12.8 μm [Ne II] fine structure line. A high quality near-IR spectrum was presented by *Martín-Hernández et al.* (2003) which allowed a more accurate comparison with the surrounding molecular gas through the presence of the H_2 S(1) line. Its velocity agreed well with millimetre molecular line measurements even though it is likely to arise in a thin layer just outside the ionized zone.

Comparison with the molecular cloud velocity is a vital part of testing dynamical models since it sets the reference frame. For instance, in G29.96-0.02, where the tail is clearly pointing towards us, the bow shock model would predict that most of the gas is redshifted as the stellar wind shock tunnels into the molecular cloud. At the other extreme, a pure champagne fbw scenario would involve most of the gas being blueshifted as it photo-evaporates off the molecular cloud face and fbws back down the density gradient towards the observer. In G29.96-0.02, and other simple cometary objects where sufficiently good spatially resolved velocity data for the ionized and molecular gas exists (e.g., *Keto et al.*, 1995; *Garay et al.*, 1994; *Hoare et al.*, 2003; *Cyganowski et al.*, 2003), the range of velocity structure usually straddles the molecular cloud velocity.

As discussed in Section 2.3, stellar winds must be included in any realistic model of expanding H II regions. The limb-brightened morphology in the ionized gas of the shell and cometary regions gives the appearance that the central regions are cleared out by a strong stellar wind. Pure champagne fbw models (*Yorke et al.*, 1983) have a centrally peaked radio structure. Numerical modelling by *Comeron* (1997) first indicated that winds can produce limb-brightened cometary structures. The action of the wind also helps to slow the expansion, as the ionization front is trapped in the dense swept up shell, as first pointed out by *Turner and Matthews* (1984). The spherically symmetric wind-driven H II region models by *González-Aviles et al.* (2005) produced very thin shell nebular regions. They found that when the H II region is expanding into a logatropic density distribution $\rho \propto r^{-1}$, driven by stellar winds with mass-loss rates $\dot{M}_w \sim 10^{-5}$ $M_\odot yr^{-1}$ and wind speeds, $v_w \sim 1000$ km s^{-1}, the H II shells evolve from HCHII to UCHII sizes in timescales $\Delta t \sim 3 - 7 \times 10^4$ yr.

Recently, new hydrodynamical models of cometary H II regions by *Arthur and Hoare* (2006) considered the action of fast ($\sim$2000 km s^{-1}), strong ($\dot{M} \sim 10^{-6}$ $M_\odot$) winds, typical for early type stars, within steep power-law and exponential density gradients. Fig. 4 (left) shows the emission measure map from one such model that has a limb-brightened structure very much like those seen in cometary objects. If the mass-loss rate is dropped by an order of magnitude then the wind can no longer open up a significant cavity.

In these champagne models with a stellar wind, the ionized gas is forced to fbw in a parabolic shell around the bubble blown by the stellar wind and then on down the density gradient. To achieve the right velocity structure relative to the molecular cloud a bow shock element is also required, whereby the star is moving up the density gradient. A stellar speed in the range 5-10 km s^{-1} is sufficient to provide enough forward motion of the gas in the head to shift those velocities relative to the molecular cloud by the typical amount observed. Fig. 4 (right) shows the velocity structure for such a combined champagne and bow shock model. This model produces a velocity structure similar to that seen in G29.96-0.02 (Fig. 5). Such a hybrid between pure champagne and pure bow shock models was also developed by *Cyganowski et al.* (2003) to explain the twin cometary regions in the same molecular cloud in DR21. The lifetimes predicted by such models are determined by how fast the ionisation front or the star reaches the local density maximum. For G29.96-0.02 and the DR21 regions the density maximum is of order 0.1 pc ahead of the ionisation front. For ionisation fronts advancing at about 3 km s^{-1} as in the *Arthur and Hoare* (2006) models this gives a lifetime of a few times 10^4 years, similar to the timescale for the star to reach the same point. *Kawamura and Masson* (1998) measured the expansion speed of the cometary W3(OH) region to be 3-5 km s^{-1}.

Zhu et al. (2005) developed a model of fbw around a parabolic shell for the G29.96-0.02 and Mon R2 cometary regions including pressure gradient forces resulting from the sweeping up of material by the bow shock, but still within a constant ambient density. As with the original bow shock models for G29.96-0.02, this required a stellar velocity of 20 km s^{-1} resulting in a mis-match with the molecular cloud reference frame of 10 km s^{-1}. *Lumsden and Hoare* (1996, 1999) also needed to invoke a 10 km s^{-1} shift in the opposite direction to get their semi-empirical champagne fbw model to agree with the observations, which they ascribed to expansion of the ionization front. Overall, the picture that is emerging for the few well-studied cometary regions is that the morphology, velocity structure and lifetime of cometary UCHII regions can be explained by a combination of champagne fbw down a density gradient and bow

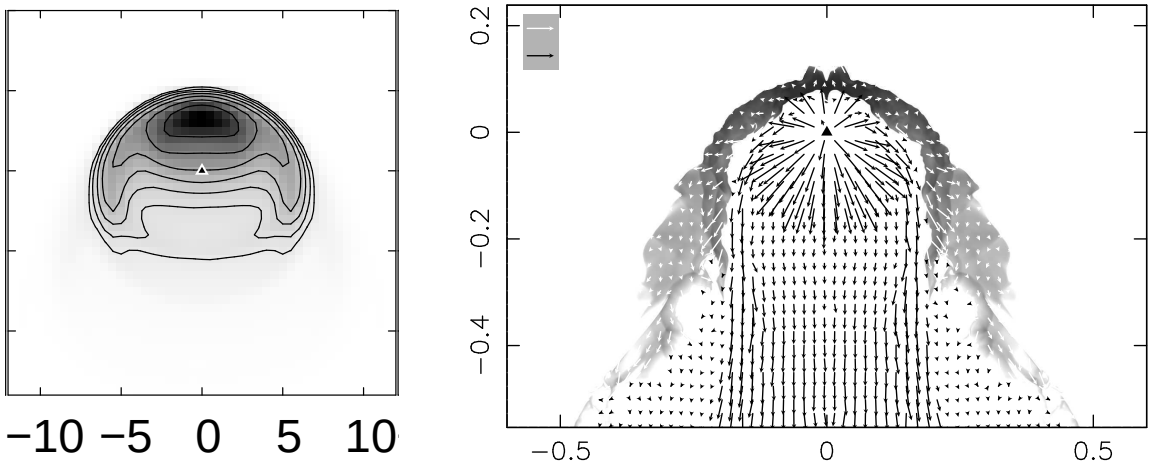

Fig. 4.— Results from hydrodynamic modelling of a cometary UCHII region expanding into an exponential density gradient of scale height 0.2 pc excited by a star with stellar wind typical for an early type star and moving up the density gradient by 10 km s^{-1}. Left: Predicted emission measure map at age 20 000 years with size scale in arcseconds for an adopted distance of 7 kpc. Right: Corresponding velocity structure of the model with white arrows showing velocities up to 30 km s^{-1} and black arrows up to 2000 km s^{-1}. The ionisation front at the head moves up the density gradient at about 3 km s^{-1}. From *Arthur and Hoare* (2006).

shock motion up the density gradient. This still remains to be tested on a wider range of objects. Possible explanations of the direction of motion will be discussed by *Hoare et al.*, in preparation.

3. HYPER-COMPACT H II REGIONS

3.1 Observed Properties

Within the large number of UCHII regions that have been discovered, a number of objects stand out as being exceptionally small and dense. Sizes for this group are ≤ 0.05 pc (10,000 AU) while densities are $\geq 10^6$ cm^{-3} and emission measures are $\geq 10^{10}$ pc cm^{-6}. In the past few years, these regions have come to be considered as a separate class, referred to as *hyper-compact* H II regions (HCHII). These regions are considered a distinct class from UCHII regions — rather than merely representing the most extreme sizes and densities — primarily because they have extremely broad radio recombination line profiles, with ΔV typically 40 – 50 km s^{-1}, and some greater than 100 km s^{-1} (*Gaume et al.*, 1995; *Johnson et al.*, 1998; *Sewilo et al.*, 2004). By comparison, UCHII regions typically have recombination line widths of 30 – 40 km s^{-1} (*Keto et al.*, 1995; *Afflerbach et al.*, 1996). Although the precise relationship between HCHII regions and Broad Recombination Line Objects (BRLO) is not yet clear, at present the two classes have so many objects in common that we take them to be one and the same.

There are also similarities between the HCHII/BRLOs and the massive YSOs that have strong ionized stellar winds, including BN, W33A, Cep A2, GGD27 and S140 IRS 1 (*Rodríguez*, 1999; *Hoare*, 2002). These luminous ($> 10^4$ L$_\odot$), embedded sources are often found without hot molecular core signatures, but are usually still driving outfbws and probably accreting. We do not use the term "protostar", since it is likely that the luminosity of these objects is dominated by hydrogen burning and not accretion, which cannot be observationally distinguished at present.

The massive YSOs are weaker radio sources and have therefore not been the subject of radio recombination line studies. However, their IR recombination line profiles have been studied and are very broad, usually in excess of 100 km s^{-1} (e.g., *Bunn et al.*, 1995). High resolution radio mapping has yielded both jet and equatorial wind morphologies for the nearest sources (*Hoare*, 2002; *Patel et al.*, 2005). Proper motion studies of jet sources reveal velocities of 500 km s^{-1} (*Martí et al.*, 1998) and the high collimation suggests a magneto-hydrodynamic mechanism as in low-mass YSOs. (Note the ionized X-wind or 'outfbw-confined' model put forward for HCHII regions by *Tan and McKee* (2003) is more appropriate for these jet sources than the slower HCHII regions.) The equatorial wind sources can result from the pressure of stellar radiation acting on the gas on the surface of the accretion disk (*Sim et al.*, 2005).

A key difference between wind sources and UCHII regions is that in wind sources the ionized material originates from the star-disk system itself. In contrast, for expanding UCHII regions it is the surrounding molecular cloud material that is being ionized.

The observed properties of HCHII regions would appear to be intermediate between these two extremes, as illustrated in Fig. 6. The size versus line width plot is an extension of previous plots, e.g., *Garay and Lizano* (1999). The line widths for the MYSO wind sources are from the near-IR Brγ line, whilst those for the UCHII and HCHII regions are from radio recombination lines. The highest frequency

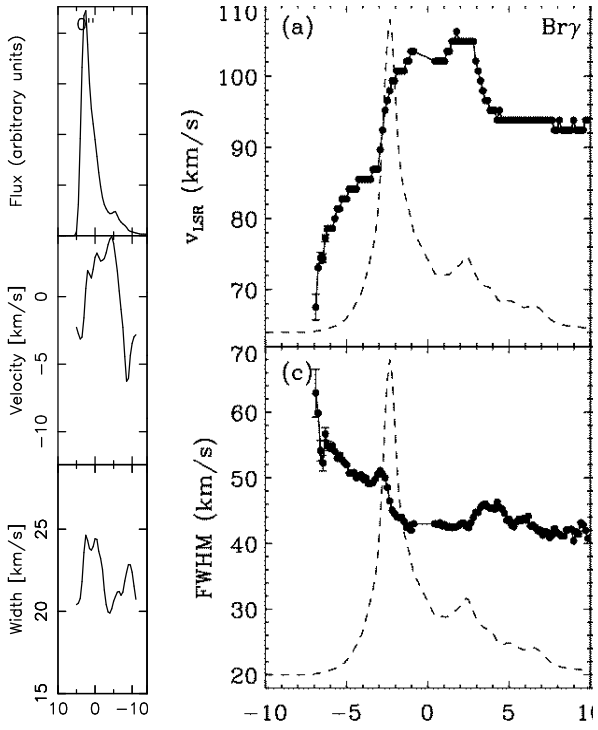

Fig. 5.— Left: Simulated long-slit spectral data along the axis of the model cometary H II region shown in Fig. 4. The three panels show the flux, velocity centroid and line width respectively. Velocities are with respect to the molecular cloud which is at rest in the simulation. Horizontal axis is offset from the position of the exciting star in arcseconds. Right: Long-slit spectral data for a position approximately along the axis of G29.96-0.02 from *Martín-Hernández et al.* (2003). Top panel shows the velocity centroid measured for the Brγ line whilst the bottom shows the observed line width with the flux profile in the dotted line. The best estimate of the ambient molecular cloud velocity is v_{LSR}=98 km s^{-1}. Horizontal axis is offset from the exciting star in arcseconds.

data available was used to minimize the effects of pressure broadening. For winds, the size varies with frequency and the measured or extrapolated size at 8 GHz is plotted. The UCHII region size does not vary with frequency and we assume the same for HCHII regions, although they may vary somewhat.

For the right-hand plot of the radio brightness normalised to the total luminosity, the HCHII and UCHII regions are clearly much more radio-loud than the MYSO winds. The 8 GHz radio luminosity is not a straightforward property to use, because it under-estimates the number of ionizing photons produced by the exciting source when the source is optically thick. At 8 GHz, HCHII regions in particular, are well below their turnover frequency, and present correspondingly lower flux densities. There is also a strong dependence on the effective temperature of the ionizing source. It should be noted that the MYSO wind sources plotted (BN, W33A, S140 IRS 1, NGC 2024 IRS 2, GL 989 and GL 490) are somewhat lower luminosity than most of the H II regions plotted. However, the combination of these observable parameters provides a reasonable indication as to what type of object one is dealing with. It is interesting to note that NGC 7538 IRS 1 stands out in these plots as an exceptional source due to its broad lines and strong emission.

Two different physical mechanisms may contribute to the broad line-widths of HCHII regions. Pressure broadening can be significant in such high density regions, particularly for the high principle quantum number centimeter wave transitions observed with the VLA, owing to the n^7 dependence of the broadening (e.g., *Brocklehurst and Seaton*, 1972; *Griem*, 1974; see also *Keto et al.*, 1995 for a discussion of the combination of dynamics and line broadening as applied to H II regions). Bulk motion of the gas, either via accretion (e.g., *Keto*, 2002b, *Keto and Wood*, 2006), outflow (e.g., *Lugo et al.*, 2004), or rotation, could be occurring. To distinguish the relative contributions from pressure broadening and bulk motion of the gas will require high spatial resolution ($\leq 1''$) observations over a wide range of frequencies, including low principal quantum number transitions in the millimeter, sub-millimeter and IR regions.

Apart from the common occurrence of broad recombination lines, other differences exist between the hyper- and ultra-compact classes. UCHII regions typically have turnover frequencies (between the optically thick and thin regimes) of 10 – 15 GHz, while HCHII regions become optically thin at frequencies above 30 GHz, owing to their higher densities. Nevertheless, no HCHII regions have been found with an optically thick spectral index of +2, indicative of uniform density gas. Rather, HCHII regions show an intermediate spectral index of $\sim +1$ which suggests non-uniform gas density. Some UCHII regions also show $\alpha \sim +1$ at centimeter wavelengths. Density gradients have been invoked to explain these intermediate spectral indices (e.g., *Franco et al.*, 2000; *Avalos et al.*, 2005). Although a density gradient and small size are suggestive of a stellar wind, the measured flux densities and the inferred electron densities are much higher than values encountered in stellar winds. A disk wind, however, may be capable of producing a density gradient, and at the high electron densities implied by the radio flux densities (*Lugo et al.*, 2004; see §3.2). The effect of champagne flows or influence of stellar gravity (Keto 2003) lead to steep density gradients. *Ignace and Churchwell* (2004) have shown that the intermediate spectral indices can also be produced by unresolved clumps with a power-law distribution of optical depths.

Morphologies of HCHII regions are not well-known; to date, only a few have been resolved by radio continuum observations. The archetypal BRLO NGC 7538 IRS 1 is bipolar, but other morphologies are seen as well. Fig. 7 shows radio continuum images of NGC 7538 IRS 1, M17-UC1, and G28.20−0.04 which have, respectively, bipolar, cometary and shell-like morphologies. The high spatial resolution observations needed to identify the nature of the broad recombination line emission will also provide much-needed morphological information.

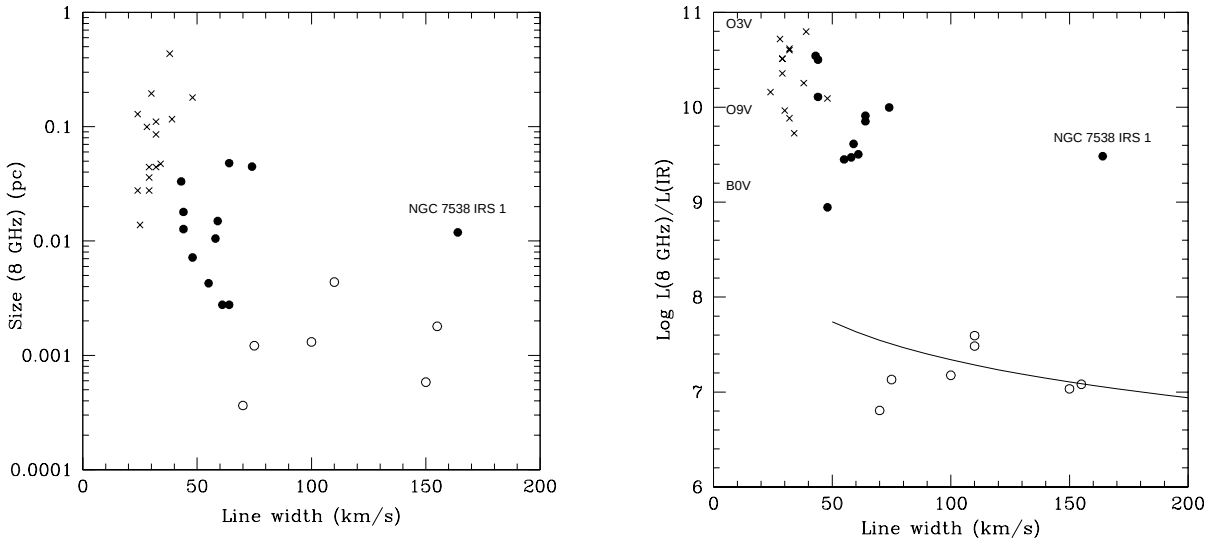

Fig. 6.— Left: Size versus line width for UCHII regions (crosses), HCHII regions (solid circles) and massive young stellar object wind sources (open circles). Line widths are FWHM. Sizes are measured or equivalent at 8 GHz and are geometric mean FWHM. Note how the HCHII regions lie between UCHII regions and the MYSOs wind sources. Right: As left, but for the ratio of the radio luminosity at 8 GHz (W Hz^{-1}) to the bolometric luminosity from the IR ($L_\odot$) (except W49A regions where radio spectral type has been used). The flux at 8 GHz has been extrapolated from higher frequencies if not measured directly, using observed or typical spectral indices. Data for UCHIIs are from *Wood and Churchwell* (1989a) and *De Pree et al.* (2004); for the HCHII regions from *Sewilo et al.* (2004), *Jaffe and Martin-Pintado* (1999), *Johnson et al.* (1998), and *De Pree et al.* (2004); and for the MYSO wind sources from *Bunn et al.* (1995) and *Nisini et al.* (1994). Sizes of MYSOs come from *Hoare* (2002) and references therein; *Rengarajan and Ho* (1996); *Snell and Bally* (1986); *Campbell et al.* (1986). The expected ratio for optically thin H II regions for given spectral type exciting stars is indicated at top left using stellar parameters from *Smith et al.* (2002). The solid line shows the level expected for a stellar wind assuming $\dot{M}$=10^{-6} $M_\odot$ yr^{-1}, $v_{\rm inf} = 2v_{FWHM}$ and L(bol)=10^4 $L_\odot$ (*Wright and Barlow*, 1975).

Although classifications based on observed parameters can be useful, a more fundamental definition relating to the nature of the object is preferable. One possibility is to define HCHIIs as those regions with radii less than the transonic point where the escape velocity from the star(s) within the H II region equals the ionized gas sound speed (see §3.2). Alternatively, one might consider the place of HCHIIs in the general massive star formation process. In this context, the crucial element is the recognition that HCHII sizes are 10,000 AU *and smaller*. Regardless of the model of massive star formation that is adopted, it is clear that HCHII sizes are approaching a scale appropriate for individual high mass star formation.

3.2 Theoretical Models

3.2.1 Context - Hot Molecular Cores The observed properties of the HCHII regions suggest that they are very young and it is natural to associate them with the turn-on of the Lyman continuum radiation. H II regions around stars later than early-B type are not detectable by present radio telescopes. Thus, if a star is growing by accretion through the spectral type sequence from B to O (see §3.2.2), then in the earlier stages the star and accretion flow would appear as a hot molecular core (HMC) without radio continuum emission. *Osorio et al.* (1999) modelled the spectral energy distribution of the thermal emission from dust in such HMCs accreting toward a central star. They modelled the HMCs as logatropic cores with pressure $P = P_0 \log(\rho/\rho_{\rm ref})$, where $P_0 \sim 10^{-7} - 10^{-6}$ dynes cm^{-2} is the pressure constant and $\rho_{\rm ref}$ is a reference density (*Lizano and Shu*, 1989; *Myers and Fuller*, 1992). Logatropic cores have an equilibrium density profile $\rho \propto r^{-1}$, and a large velocity dispersion $\sigma^2 = dP/d\rho = P_0/\rho$, that increases with decreasing density, as observed in molecular clouds (e.g., *Fuller and Myers*, 1992) supporting massive envelopes of several hundred $M_\odot$. The gravitational collapse of logatropic spheres has the property that the mass accretion rate increases with time as $\dot{M} \propto t^3$ (*McLaughlin and Pudritz* 1997). In a comparison of their model with observations of several hot molecular cores without detectable radio continuum *Osorio et al.* found that the observed spectral energy distributions (SEDs) were consistent with central B stars with ages $\tau_{\rm age} \lesssim 6 \times 10^4$ yr, accreting at rates of $\dot{M}_{\rm acc} > 10^{-4}\, M_\odot\, {\rm yr}^{-1}$. At these accretion rates, the main heating agent is the luminosity arising from the deceleration of the accretion flow, $L_{\rm acc} = GM_*\dot{M}_{\rm acc}/R_*$ (assuming purely spherical accretion). Comparison of observed

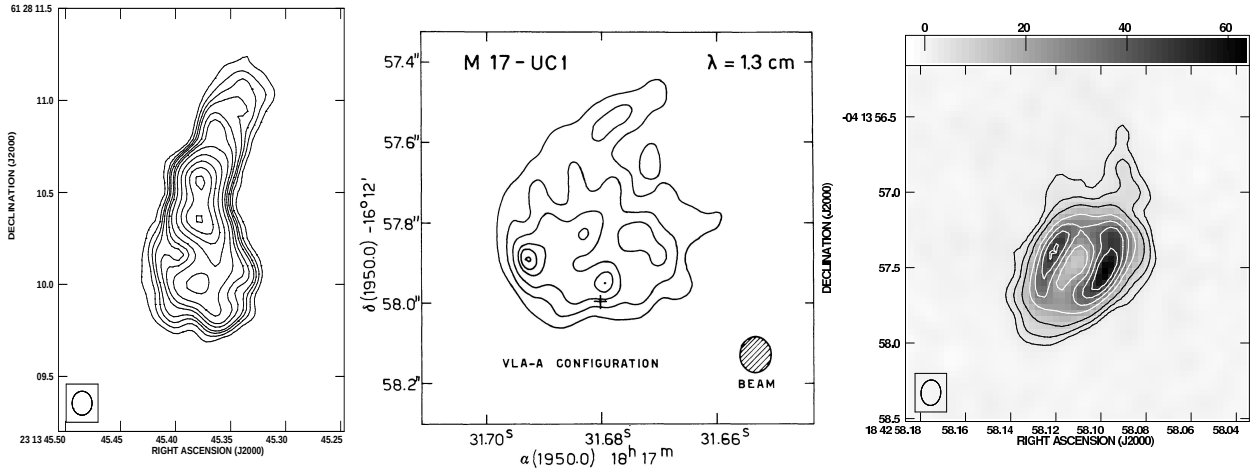

Fig. 7.— The different morphologies of hyper-compact H II regions. Left: the bipolar NGC 7538 IRS 1 (*Franco-Hernández and Rodríguez*, 2004), Middle: the cometary M17 UC1 (*Felli et al.*, 1984) and Right: the shell-like G28.20−0.04 (*Sewilo et al.*, 2005).

and modeled SEDs suggests that some HMCs are consistent with the earlier stages of the formation of massive stars by accretion.

The logatropic core model is also attractive because it has properties that are required if massive stars are to form despite the constraints imposed by the outward force of radiation pressure and within the short time scale allowed by the main sequence lifetime. *Osorio et al.* showed that their inferred accretion rates were large enough that the momentum of the accretion flow could overcome the outward force of radiation pressure on dust grains. At the risk of oversimplicity, this argument may be summarised as follows: The most naive estimate of the outward force deriving from the luminosity, assuming spherical geometry and the total absorption of the luminosity by the dust in the flow, would be L/c. A similarly simple estimate of the force deriving from the momentum of the accretion flow, again assuming spherical accretion, is $\dot{\mathrm{M}}v$. If the momentum of the accretion flow is high enough, the flow will push the dust grains inward until they are sublimated by the higher temperatures in the center of the flow. At this point the flow is rendered essentially transparent to the stellar radiation (*Kahn*, 1974; *Wolfire and Cassinelli*, 1987).

3.2.2 Ionized Accretion Flow or Gravitationally Trapped H II regions Once the star, possibly one of the several stars forming together, has gained sufficient mass and therefore temperature, the number of emitted Lyman continuum photons will be enough to ionize an H II region within the continuing accretion flow. The radius of ionization equilibrium, r_i, is set by the balance between ionization and recombination within the H II region. If r_i is less than the gravitational radius in the accretion flow, $r_g \equiv GM_\star/a^2$, where the inward velocity equals the sound speed of the ionized gas, a (within a factor of 2), then the H II region can be trapped within the accretion flow with its boundary as a stationary R-type ionization front. This model explains why the development of an HII region does not immediately end the accretion as would be expected in the classic textbook model for the evolution of H II regions by pressure driven expansion (*Shu*, 1992; *Spitzer*, 1978; *Dyson and Williams* 1980). In pressure driven expansion, the flow of the ionized gas is entirely outward, precluding accretion. The model for H II regions trapped within an accretion flow was developed to explain the observations of the inward flow of ionized gas toward the massive stars forming in the H II region G10.6–0.4 (*Keto*, 2002a).

The accretion model assumed in *Keto* (2002b) is a spherical steady-state flow (Bondi accretion) which has a density gradient everywhere less steep than $n \sim r^{-3/2}$. This is significant in that the spherical solution for ionization equilibrium does not allow for solutions in steeper density gradients (*Franco, Tenorio-Tagle and Bodenheimer*, 1990). Similar to accretion in a logatropic sphere, Bondi accretion has the property that the accretion rate depends on the stellar mass (as M^2 in Bondi accretion). As in the model of *Osorio et al.* (1999), this model relies on the momentum of a massive accretion flow to overcome the radiation pressure of the stars. Observations of G10.6–0.4 indicate that the outward force from the observed luminosity of 1.2×10^6 $\mathrm{L}_\odot$ (*Fazio et al.*, 1978) is approximately equal to the inward force deriving from the momentum of the flow, $\dot{\mathrm{M}}v \sim 3 \times 10^{28}$ dynes, for an estimated accretion rate of 10^{-3} $\mathrm{M}_\odot$ yr^{-1} and velocity of 4.5 km s^{-1} at 5000 AU (*Keto*, 2002a). In this model, the accretion flow, if not reversed by radiation pressure, will end when the ionization rate, which increases with the increasing mass of the star(s), is high enough that the radius of ionization equilibrium increases beyond the gravitational radius.

While the central star is accreting mass at rates $\dot{M} \sim 10^{-3}$ $M_{\odot}yr^{-1}$, the ram pressure of the accreting material will be larger than the ram pressure of the stellar wind, $\rho_{\rm acc} v_{\rm acc}^2 >> \rho_{\rm w} v_{\rm w}^2$, and will prevent the stellar wind from blowing out. If the radiation pressure on dust grains reverses the accretion flow, or the HCHII region expands because its radius becomes larger than r_g, then a stellar wind can blow out (see also *González-Avilés et al.*, 2005).

Recently, *Keto and Wood* (2006) extended the model of *Keto* (2002b) to consider accretion flows with angular momentum as described by *Ulrich* (1976) and *Terebey et al.* (1984). In this model of accretion, the gas spirals in to the star on ballistic trajectories conserving angular momentum. An accretion disk develops at a radius r_D, where the centrifugal force balances the gravitational force, $\Gamma^2/r_D^3 = GM/r_D^2$, roughly where the infall velocity equals the rotational velocity. Here Γ is the initial specific angular momentum. Since $r_D \sim GM/v_{orbital}^2$, if $v_{orbital} < c$ at the gravitational radius, r_g, then the radius of disk formation will be within the maximum radius, r_g, of a trapped H II region. Thus the radius of disk formation, depending on the flux of ionizing photons, could be within the ionized portion of the flow, meaning that the accretion disk would form out of infalling ionized gas. Note that the central parts of the centrifugal disk should be neutral because the gas recombines at the high densities expected in these disks. With a different choice of parameters, specifically, if the ionizing photon flux or the angular momentum were greater than in the previous case, then the disk might form in the molecular portion of the flow. In this case, the accretion flow would have the same structure as that assumed in the model of photo-evaporating disks of *Hollenbach et al.* (1994) and *Johnstone et al.* (1998).

Keto and Wood (2006) proposed the following evolutionary hypothesis for the development of an H II region within an accretion flow with a disk that parallels the development of an H II region within a spherical accretion flow. In the initial stage when there is no H II region, necessarily $r_D > r_i$ and the flow is described by the massive molecular accretion disk. In the second stage, a trapped HCHII region will develop in the center of the disk. Because the gas in the disk is denser than the gas elsewhere around the star, the molecular accretion disk will not necessarily be fully ionized, but because $r_i < r_g$, the ionized surface of the disk will not be expanding off the disk. Rather there will be a limited region, contained within the H II region, with an ionized accretion flow onto the disk. However, depending on the initial angular momentum in the flow, this region may be very small with respect to the extent of the molecular disk. Outside this region, there will be a molecular accretion flow onto the disk. The third stage of evolution is defined by the condition $r_{ionized} > r_G$. In the non-spherical case, because the gas density around the star is a function of angle off the disk, the ionization radius, r_i will also be a function of angle. If the disk is sharply defined as in the *Ulrich* (1976) and *Terebey et al.* (1984) models, then in the third stage the H II region will expand around the disk. In this third stage, because $r_i > r_g$, the surface of the disk (except for a small region in the center) will photo-evaporate with an outward flow of ionized gas off the disk, as described in the models for photo-evaporating disks.

3.2.3 Photoevaporating Disks Hollenbach et al. (1994) and *Johnstone et al.* (1998) proposed that unresolved UCHII (now termed HCHII regions) arise from photo-evaporating molecular disks. The photo-evaporation of circumstellar molecular disks around massive stars occurs as the disk surface is ionized by the stellar Lyman continuum photons. *Hollenbach et al.* proposed that within the gravitational radius, r_g, the heated gas is confined in the gravitational potential well of the star. For $r > r_g$ the ionized gas can escape and an isothermal evaporative flow is established. The ionized material flows away, but is constantly replenished by the photo-evaporation of the disk. If the star has a strong stellar wind, the wind may push the confined gas within r_g out to a critical radius where the ram pressure of the stellar wind is balanced by the thermal pressure of the photo-evaporated flow, resulting in outflow at all radii. *Yorke and Welz* (1996) and *Richling and Yorke* (1997) made hydrodynamical simulations of the evolution of photo-evaporated disks under a variety of conditions. In particular, *Richling and Yorke* found that scattering of ionizing photons on dust grains increases the photo-evaporation rate.

Recently, *Lugo et al.* (2004) modeled the density and velocity structure of axisymmetric isothermal winds photo-evaporated from a spatially thin Keplerian disk. They calculated the predicted free-free continuum emission of these models to match the observed spectral energy distributions of the bipolar objects MWC 349 A and NGC7538 IRS 1. These models naturally give a bipolar morphology which is seen in a subset of the HCHII regions. The next step is to investigate whether the thermally evaporating flow can produce the high velocities seen in the broad recombination line objects.

4. FUTURE DIRECTIONS

A key test of all the proposed models for the HCHII regions and broad recombination line objects is to match the observed morphologies and velocity structures of the ionized gas. Quality datasets already exist for a few well-studied examples against which to test the models. At present there are so few objects that a wider sample is needed to determine whether well-defined morphological classes actually exist. This may be challenging since they do appear rare, presumably since the phase is short-lived, but it does mark an important transition. Further high frequency radio recombination line observations and, where possible, IR spectroscopy, are needed to separate those that are merely pressure broadened (and therefore likely to be understood in terms of the usual UCHII region dynamics) from those that need a new physical picture. We also eagerly await the results currently being obtained with the sub-millimeter array (SMA) and the future studies that will

be made with the millimeter interferometers CARMA and ALMA. These will be able to trace the molecular gas dynamics down to the scales of the HCHII regions.

Once the ionization front expands to UCHII region scales, it is likely to leave behind the local density enhancement resulting from the gravitational collapse and begin to experience the wider environment in which the collapse took place. Significant proper motion relative to the cloud core will add to this effect. The presence of champagne flows in cometary H II regions indicates that the wider environment must have a density gradient, i.e. the cometary regions are not located at the core center. The original blister picture developed by *Israel* (1978) argued that such regions are a result of triggered star formation rather than spontaneous collapse; the latter more likely to occur within a dense core. He was considering more evolved H II regions, but they show a similar distribution of morphological types as the UCHII regions (*Fich*, 1993). Velocity studies of large, optically visible H II regions have revealed that champagne flows dominate their dynamics too (e.g., *Priestley*, 1999, *Roger et al.*, 2004). This is most easily understood as the continued evolution of cometary UCHIIs down a large scale density gradient.

A key test of the dynamical models for cometary regions is to measure the motion of the stars. Radial velocity measurements on the star in G29.96-0.02 were attempted by *Martín-Hernández et al.* (2003). However, the resolution and signal-to-noise of the spectrum, and uncertainties in the rest wavelengths of the heavy element spectral features uncontaminated by nebular lines, prevented the required precision. Once the EVLA and e-MERLIN telescopes come on-line it may be possible to detect the radio emission directly from the free-flowing stellar wind of the exciting stars at high resolution. This would open up the possibility of proper motion measurements directly on the stars, as well as many more expansion measurements of the nebulae themselves.

The more global aspects of massive star formation will be addressed by the numerous galactic plane surveys in coming years, following the lead by the GLIMPSE survey in the mid-IR. A high resolution radio survey of the entire northern GLIMPSE region (www.ast.leeds.ac.uk/Cornish) will pick out all UCHII regions across the galaxy, building on the previous blind surveys by *Giveon et al.* (2005) and references therein. These will be complemented by a sub-millimetre continuum survey of the plane at the JCMT, methanol maser surveys using Parkes and the Lovell telescopes (www.jb.man.ac.uk/research/methanol), ^{13}CO from the BU-FCRAO Galactic Ring Survey (www.bu.edu/GRS), H I from the VLA survey (www.ras.ucalgary.ca/VGPS) and near-IR from UKIRT (www.ukidss.org).

Unbiased area surveys will allow the luminosity function and lifetimes to be derived and compared with simulations of the evolution of the Galactic UCHII region population. Their location within the wider GMCs, the fractions that appear to be triggered or isolated and their location relative to potential external triggers will be established on a large scale statistical basis. The power of this sensitive, multi-wavelength, high resolution campaign on the Milky Way will yield many advances in our understanding of massive star formation.

Acknowledgements. We would like to thank Jane Arthur for her input on the hydrodynamic modelling and James Urquhart and Ant Busfield for help with the figures. Useful discussions were had with Tom Hartquist and Jim De Buizer. We thank the referee for several useful suggestions.

REFERENCES

Afflerbach A., Churchwell E., Hofner P., and Kurtz S. (1994) *Astrophys. J., 437*, 697-704.
Afflerbach, A. et al., (1996) *Astrophys. J. Supp., 106*, 423-446.
Alvarez, C. et al., (2004) *Astrophys. J. Supp., 155*, 123-148.
Arthur J. and Hoare M. G. (2006) *Astrophys. J.*, submitted.
Avalos M., Lizano S., Rodríguez L., Franco-Hernández R., and Moran J. (2006) *Astrophys. J.*, in press.
Benjamin R. A. et al. (2003) *Publ. Astron. Soc. Pac., 115*, 953-964.
Bik A., Kaper L., Hanson M. M., and Smits M. (2005) *Astron. Astrophys., 440*, 121-137.
Bourke T. L., Hyland A. R., and Robinson G. (2005) *Astrophys. J., 625*, 883-890.
Brocklehurst M. and Seaton M. J. (1972) *Mon. Not. R. Astron. Soc., 157*, 179-210.
Bunn J. C., Hoare M. G., and Drew J. E. (1995) *Mon. Not. R. Astron. Soc.*, 272, 346-354.
Calvet N. et al., (2004) *Astron. J., 128*, 1294-1318.
Campbell B., Persson S. E., and McGregor P. J. (1986) *Astrophys. J., 305*, 336-352.
Cesaroni R., Churchwell E., Hofner P., Walmsley C. M., and Kurtz S. (1994) *Astron. Astrophys., 288*, 903-920.
Cesaroni R., Walmsley C. M, and Churchwell E. (1992) *Astron. Astrophys., 256*, 618-630.
Churchwell E. (1999) In *The Origin of Stars and Planetary Systems* (C. Lada and N. Kylafis, eds.), pp. 515-552. NATO Science Series, Kluwer, The Netherlands.
Churchwell E. (2002) *Ann. Rev. Ast. Astrophys.*, 40, 27-62.
Codella C., Felli M., and Natale V. (1994) *Astron. Astrophys., 284*, 233-240.
Comeron F. (1997) *Astron. Astrophys., 326*, 1195-1214.
Cyganowski C. J., Reid M. J., Fish V. L., and Ho P. T. P. (2003) *Astrophys. J. 596*, 344-349.
De Buizer J. M., Radomski J. T., Pia R. K., Telesco C. M. (2002b) *Astrophys. J., 580*, 305-316.
De Buizer J. M., Radomski J. T., Telesco C. M., and Pia R. K. (2003) *Astrophys. J., 598*, 1127-1139.
De Buizer J. M., Radomski J. T., Telesco C. M., and Pia R. K. (2005) *Astrophys. J. Supp, 156*, 179-215.
De Buizer J. M., Watson A. M., Radomski J. T., Pia R. K., and Telesco C. M. (2002a) *Astrophys. J., 564*, L101-L104.
De Pree C. G., Rodríguez L. F., and Goss W. M.. (1995) *Rev. Mex. Astron. Astrophys., 31*, 39-44.
De Pree C. G. et al. (2004) *Astrophys. J., 600*, 286-291.
De Pree C. G., Wilner D. J., Deblasio J., Mercer A. J., and Davis L. E. (2005) *Astrophys. J., 624*, L101-104.

De Wit W. J., Testi L., Palla F., and Zinnecker H. (2005) *Astron. Astrophys., 437*, 247-255.
Dickel H. R. and Goss W. M. (1987) *Astron. and Astrophys., 185*, 271-282.
Dickel H. R., Goss W. M., and De Pree C. G. (2001) *Astron. J., 121*, 391-398.
Draine B. T. (2003) *Ann. Rev. Astron. Astrophys., 41*, 241-289.
Dyson J. and Williams D. (1980) *The Physics of the Interstellar Medium*, Wiley, New York.
Dyson J., Williams R., and Redman M. (1995) *Mon. Not. R. Astron. Soc., 227*, 700-704.
Ellingsen S. P., Shabala S. S., and Kurtz S. E. (2005) *Mon. Not. R. Astron. Soc., 357*, 1003-1012.
Fazio G. G. et al. (1978) *Astrophys. J., 221*, L77-81.
Feldt M., Stecklum B., Henning Th., Launhardt R., and Hayward T. L. (1999) *Astron. Astrophys., 346*, 243-259.
Felli M., Churchwell E., and Massi M. (1984) *Astron. Astrophys., 136*, 53-64.
Fey A. L., Gaume R. A., Claussen M. J., and Vrba F. J. (1995) *Astrophys. J., 453*, 308-312.
Fich M. (1993) *Astrophys. J. Supp., 86,*, 475-497.
Franco J., et al. (2000) *Astrophys. J., 542*, L143-146.
Franco J., García-Segura G., and Kurtz S. E (2006) *Astrophys. J.*, submitted.
Franco J., Shore S. N., and Tenorio-Tagle G. (1994) *Astrophys. J., 436*, 795-799.
Franco J., Tenorio-Tagle G., and Bodenheimer P. (1990) *Astrophys. J., 349*, 126-140.
Franco-Hernńdez R. and Rodríguez L. F. (2004) *Astrophys. J., 604*, L105-108.
Fuller G. A. and Myers P. C. (1992) *Astrophys. J., 384*, 523-527.
Garay G. and Lizano S. (1999) *Publ. Astron. Soc. Pac., 111*, 1049-1087.
Garay G., Gómez Y., Lizano S., and Brown R. L. (1998b) *Astrophys. J., 501*, 699-709.
Garay G., Lizano S., and Gómez Y. (1994) *Astrophys. J., 429*, 268-284.
Garay G., Lizano S., Gómez Y., and Brown R. L. (1998a) *Astrophys. J., 501*, 710-722.
García-Segura G. and Franco J. (1996) *Astrophys. J., 469*, 171-188.
Gaume R., Goss W., Dickel H., Wilson T., and Johnston K. (1995) *Astrophys. J., 438*, 776-783.
Giard M., Bernard J. P., Lacombe F., Normand P., and Rouan D. (1994) *Astron. Astrophys., 291*, 239-249.
Gies D. R. (1987) *Astrophys. J. Supp., 64*, 545-563.
Giveon U., Becker R. H., Helfand D. J., and White R. L. (2005) *Astron. J., 129*, 348-354.
Gómez L., et al. (2005) *Astrophys. J., 635*, 1166-1172.
Gómez Y., et al. (1998) *Astrophys. J., 503*, 297-306.
Gonzáles-Aviles M., Lizano S., and Raga A. C. (2005) *Astrophys. J., 621*, 359-371.
Griem H. R. (1974) *Spectral Line Broadening by Plasmas*, Academics, New York.
Hatchell J. and van der Tak F. F. S. (2003) *Astron. and Astrophys., 409*, 589-598.
Hatchell J., Thompson M. A., Millar T. J., and MacDonald G. H. (1998) *Astron. Astrophys.S, 133*, 29-49.
Henning T., Schreyer K., Launhardt R., and Burkert A. (2000) *Astron. Astrophys., 353*, 211-226.
Hoare M. G. (2002) In *Hot Star Workshop III: The Earliest Stages of Massive Star Birth*, (P. A. Crowther, ed.), p137-144. ASP Conf. Ser. 267, San Francisco.
Hoare M. G., et al. (2004) In *Milky Way Surveys: The Structure and Evolution of our Galaxy* (D. Clemens, R. Shah, and T. Brainerd, eds.), pp.156-158. Proc. of ASP Conf., 317, San Francisco: ASP.
Hoare M. G., Lumsden S. L., Busfield A. L., Buckley P. 2003 In *Winds, Bubbles and Explosions* (S. J. Arthur and W. J. Henney, eds.), pp. 172-174. Rev. Mex. Astron. Astrophys. Ser. Conf. 15.
Hoare M. G., Roche P. F., and Glencross W. M. (1991) *Mon. Not. R. Astron. Soc., 251*, 584-599.
Hofmann K.-H., Balega Y. Y., Preibisch T., and Weigelt, G. (2004) *Astron. Astrophys., 417*, 981-985.
Hofner P. and Churchwell E. (1996) *Astron. Astrophys.S, 120*, 283-299.
Hofner P., Delgado H., Whitney B., Churchwell E., and Linz H. (2002) *Astrophys. J. 579*, L95-98.
Hofner P., Kurtz S., Churchwell E., Walmsley M., and Cesaroni R. (1996) *Astrophys. J. 460*, 359-371.
Hofner P., Kurtz S., Churchwell E., Walmsley C. M., and Cesaroni R. (1994) *Astrophys. J., 429*, L85-88.
Hofner P., Wyrowski F., Walmsley C. M., and Churchwell E. (2000) *Astrophys. J., 536*, 393-405.
Hollenbach, D., Johnstone, D., Lizano, S., and Shu, F. (1994) *Astrophys. J., 428*, 654-669.
Hoogerwerf R., de Bruijne J. H. J., and de Zeeuw P. T. (2001) *Astron. Astrophys., 365*, 49-77.
Ignace R. and Churchwell E. (2004) *Astrophys. J., 610*, 351-360.
Indebetouw R., et al. (2005) *Astrophys. J., 619*, 931-938.
Israel F. P. (1978) *Astron. Astrophys., 90*, 769-775.
Jaffe D. and Martin-Pintado J. (1999) *Astrophys. J., 520*, 162-172.
Johnson C. O., De Pree C. G., and Goss W. M. (1998) *Astrophys. J. 500*, 302-310.
Johnstone D., Hollenbach D., and Bally J. (1998) *Astrophys. J., 499*, 758-776.
Kahn F. (1974) *Astron. Astrophys., 37*, 149-162.
Kawamura J. H. and Masson C. R. (1998) *Astrophys. J., 509*, 270-282.
Keto E. R., Welch W. J., Reid M. J., and Ho P. T. P. (1995) *Astrophys. J., 444*, 765-769.
Keto E. (2002a) *Astrophys. J., 568*, 754-760.
Keto E. (2002b) *Astrophys. J., 580*, 980-986.
Keto E. (2003) *Astrophys. J., 599*, 1196-1206
Keto E. and Wood K. (2006) *Astrophys. J.*, in press.
Keto E. Welch, W., Reid, M., Ho, P. (1995) *Astrophys. J., 444*, 765-769.
Kim K.-T. and Koo B.-C. (2001) *Astrophys. J., 549*, 979-996.
Kim K.-T. and Koo B.-C. (2003) *Astrophys. J., 596*, 362-382.
Kraemer K. E. et al. (2003) *Astrophys. J., 588*, 918-930.
Kurtz S., Churchwell E., and Wood D. O. S. (1994) *Astrophys. J. Supp., 91*, 659-712.
Kurtz S., et al. (2000) In *Protostars and Planets IV* (V. Mannings V., et al., eds.), pp. 299-326. Univ.of Arizona, Tuscon.
Kurtz S. E., Watson A. M., Hofner P., and Otte B. (1999) *Astrophys. J., 514*, 232-248.
Lebrón M., Rodríguez L. F., and Lizano S. (2001) *Astrophys. J., 560*, 806-820.
Linz H., Stecklum B., Henning Th., Hofner P., and Brandl B. (2005) *Astron. Astrophys., 429*, 903-921.
Lizano S. and Shu F. H. (1989) *Astrophys. J., 342*, 834-854.
Lizano S., Cantó J., Garay G., and Hollenbach D. (1996) *Astrophys. J., 468*, 739-748.

Lugo J., Lizano S., and Garay G. (2004) *Astrophys. J., 614*, 807-817.
Lumsden S. L. and Hoare M. G. (1996) *Astrophys. J., 464*, 272-285.
Lumsden S. L. and Hoare M. G. (1999) *Mon. Not. R. Astron. Soc., 305*, 701-706.
Lumsden S. L., Hoare M. G., Oudmaijer R. D., and Richards D. (2002) *Mon. Not. R. Astron. Soc., 336*, 621-636.
Lumsden S. L., Puxley P. J., Hoare M. G., Moore T. J. T., and Ridge N. A. (2003) *Mon. Not. R. Astron. Soc., 340*, 799-812.
Mac Low M.-M., Van Buren D., Wood D. O. S., and Churchwell E. (1991) *Astrophys. J., 369*, 395-409.
McLaughlin D. E. and Pudritz R. E. (1997) *Astrophys. J., 476*, 750-765.
Martí J., Rodríguez L. F., and Reipurth B. (1998) *Astrophys. J., 502*, 337-341.
Martín-Hernández N. L., Bik A., Kaper L., Tielens A. G. G. M., and Hanson M. M. (2003) *Astron. Astrophys., 405*, 175-188.
Martín-Hernńdez N. L., Vermeij R., Tielens A. G. G. M., van der Hulst J. M., and Peeters E. (2002) *Astron. Astrophys., 389*, 286-294.
Maxia C., Testi L., Cesaroni R., and Walmsley C. M. (2001) *Astron. Astrophys., 371*, 286-299.
Mueller K. E., Shirley Y. L., Evans N. J. II, and Jacobson H. R. (2002) *Astrophys. J. Supp., 143*, 469-497.
Myers P. C. and Fuller G. A. (1992) *Astrophys. J., 396*, 631-642.
Natta A. and Panagia N. (1976) *Astron. Astrophys., 50*, 191-211.
Nisini B., Smith H. A., Fischer J., and Geballe T. R. (1994) *Astron. Astrophys., 290*, 463-472.
Okamoto Y., et al. (2003) *Astrophys. J., 584*, 368-384.
Olmi L. and Cesaroni R. (1999) *Astron. Astrophys., 352*, 266-276.
Olmi L. et al. (2003) *Astron. Astrophys., 407*, 225-235.
Osorio M., Lizano S., and D'Alessio, P. (1999) *Astrophys. J., 525*, 808-820.
Patel N. A. et al. (2005) Nature, 437, 109-111.
Pratap P., Megeath S. T., and Bergin E. A. (1999) *Astrophys. J., 517*, 799-818.
Priestley C. (1999) PhD Thesis, University of Leeds.
Ramesh B. and Sridharan T. K. (1997) *Mon. Not. R. Astron. Soc., 284*, 1001-1006.
Redman M., Williams R., and Dyson J. (1998) *Mon. Not. R. Astron. Soc., 298*, 33-41.
Rengarajan T. N. and Ho P. T. P. (1996) *Astrophys. J., 465*, 363-370.
Richling S. and Yorke H. W. (1997) *Astron. Astrophys., 327*, 317-324.
Rodríguez L. F. (1999) in Star Formation 1999, Ed. T. Nakamoto, Nobeyama Radio Observatory, p. 257-262.
Roger R. S., McCutcheon W. H., Purton C. R., and Dewdney P. E. (2004) *Astron. Astrophys., 425*, 553-567.
Roshi A., Balser D. S., Bania T. M., Goss W. M., and De Pree C. G. (2005) *Astrophys. J., 625*, 181-193.
Sewilo M., Churchwell E., Kurtz S., Goss W., and Hofner P. (2004) *Astrophys. J. 609*, 285-299.
Sewilo M., et al. (2005) In *Massive Star Birth: A Crossroads in Astrophysics*, IAU Symp. 227 (R. Cesaroni et al., eds.) Poster Proceedings
www.arcetri.astro.it/iaus227/posters/sewilo_m.pdf.
Shu F. (1992) *The Physics of Astrophysics, Volume II, Gas Dynamics*, University Science Books, Mill Valley, CA.
Shull J. M. (1980) *Astrophys. J., 238*, 860-866.
Sicilia-Aguilar A. et al. (2005) *Astron. J., 129*, 363-381.
Sim S. A., Drew J. E., and Long K. S. (2005) *Mon. Not. R. Astron. Soc., 363*, 615-627.
Smith L. J., Norris R. P. F., and Crowther P. A. (2002) *Mon. Not. R. Astron. Soc., 337*, 1309-1328.
Smith N. et al. (2000) *Astrophys. J., 540*, 316-331.
Snell R. L. and Bally J. (1986) *Astrophys. J., 303*, 683-701.
Sollins P., Zhang Q., Keto E., and Ho P. (2004) *Astrophys. J., 624*, L49-52.
Sollins P., Zhang Q., Keto E., and Ho P. (2005) *Astrophys. J., 631*, 399-410.
Spitzer L., Jr. (1978) *Physical Processes in the Interstellar Medium*, Wiley, New York.
Stecklum B. et al. (2002) *Astron. Astrophys., 392*, 1025-1029.
Tan J. C. and McKee C. F. (2003) In *Star Formation at High Angular Resolution*, IAU Symp. 221, (M. G. Burton et al., eds.), ASP, astro-ph/0309139).
Terebey S., Shu F., and Cassen P., (1984) *Astrophys. J., 286*, 529-551.
Turner B. E. and Matthews H. E. (1984) *Astrophys. J., 277*, 164-180.
Ulrich R. (1976) *Astrophys. J., 210*, 377-391.
van der Walt D. J. (1997) *Astron. Astrophys., 322*, 307-310.
Walsh A. J., Burton M. G., Hyland A. R., and Robinson G. (1998) *Mon. Not. R. Astron. Soc., 301*, 640-698.
Watson A. M. and Hanson M. M. (1997) *Astrophys. J., 490*, L165-169.
Watt S. and Mundy L. G. (1999) *Astrophys. J. Supp., 125*, 143.-160
Williams R. J. R., Dyson J. E., and Hartquist T. W. (2000) 314, 315-323.
Wolfire M. and Cassinelli. J. (1987) *Astrophys. J., 319*, 850-867.
Wood D. O. S. and Churchwell E. (1989a) *Astrophys. J. Supp., 69*, 831-895.
Wood D. O. S. and Churchwell E. (1989b) *Astrophys. J., 340*, 265-272.
Wood D. O. S. and Churchwell E. (1991) *Astrophys. J., 372*, 199-207.
Wright A. E. and Barlow M. J. (1975) *Mon. Not. R. Astron. Soc., 170*, 41-51.
Wyrowski F., Schilke P., Walmsley C. M., and Menten K. M. (1999) *Astrophys. J., 514*, L43-46.
Xie T., Mundy L. G., Vogel S. N., and Hofner P. (1996) 473, L131-134.
Yorke H. W. (1986) Ann. Rev. Astron. Astrophys., 24, 49-87.
Yorke H. W. and Welz A. (1996) *Astron. Astrophys., 315*, 555-564.
Yorke H. W., Tenorio-Tagle G., Bodenheimer P., 1983, *Astron. Astrophys., 127*, 313-319.
Zhu Q.-F., Lacy J. H., Jaffe D. T., Greathouse T. K., and Richter M. J. (2005) *Astrophys. J., 631*, 381-398.